MT28-4PoM05-02

Effect of Hf Addition to Nb on Nb_3Sn Grain Morphology under High Sn Diffusion Driving Force

Koki Asai, Tsuyoshi Yagai, and Nobuya Banno

***Abstract*—Grain refinement and performance improvements for Nb_3Sn superconducting wires are highly desired for realizing next-generation high-field magnets for the Future Circular Collider (FCC) project. The target performance is a non-Cu critical current density of 1500 A/mm^2 at 4.2 K under a 16 T field. Hf addition to Nb, which leads to Nb_3Sn grain refinement, has attracted intensive interest from the viewpoint of applicability to conventional wire manufacturing. The grain-refinement effect of Hf addition is speculated to be due to promotion of Nb_3Sn phase nucleation, which is caused by an increase of nucleation sites such as dislocations or misorientations in the parent Hf-doped Nb; the deformation-induced fine microstructure remains even at the Nb_3Sn phase formation temperature. Nevertheless, our previous study on the addition of Hf–Ta to bronze-route Nb_3Sn wires did not reveal a substantial effect on grain refinement. This lack of effect might be attributed to a smaller Sn diffusion driving force in the case of the bronze route. Therefore, we here study the Nb_3Sn phase formation behavior in the case of a higher Sn diffusion driving force using tapes with a diffusion couple of Nb and high-Sn-content Sn–Cu alloy. We prepared samples with a diffusion couple of Nb–4at%Ta–1at%Hf / Sn–10at%Cu, Nb–2at%Ti–1at%Hf / Sn–10at%Cu and conducted microstructural and microchemical analyses to evaluate the formation of Nb_3Sn during the heat treatment. Grain refinement in Hf-doped Nb_3Sn wires was confirmed under a high Sn diffusion driving force. However, the grain refinement effect was weaker than the effect expected on the basis of previous works.**

***Index Terms*— Hf–Ta addition, Hf–Ti addition, Nb_3Sn, Sn diffusion driving force.**

I. INTRODUCTION

THE Future Circular Collider (FCC) project requires a non-Cu critical current density of 1500 A/mm^2 at 4.2 K under a 16 T field for Nb_3Sn wires [1]. To achieve this challenging target, grain refinement is highly desired because the grain boundaries in Nb_3Sn act as dominant pinning centers. At present, grain refinement methods such as Hf addition to Nb [2] and the internal oxidation technique [3][4] are expected to lead to a breakthrough for the grain refinement of Nb_3Sn. Hf addition in particular is expected to be easily applicable to conventional drawing process. The deformation-induced fine grain morphology of the parent Hf-doped Nb phase has been reported to remain even at the Nb_3Sn formation temperature, which is believed to promote Nb_3Sn nucleation [5][6]. Nevertheless, our previous study showed that the addition of Hf–Ta to Nb in bronze-route Nb_3Sn did not lead to substantial grain refinement [7][8]. In addition, Bovone *et al*. have recently reported that Hf addition did not lead to substantial grain refinement in rod-in-tube-processed Nb_3Sn wires [9]. Meanwhile, Xu *et al*. have reported grain refinement by Hf addition in powder-in-tube-processed samples under conditions with no oxidation source [10]. In addition, we have recently reported a grain refinement effect by Hf through in-depth scanning transmission electron microscopy (S/TEM) observations of Ti–Hf and Ta–Hf Nb_3Sn layers [11]. Thus, the effect of Hf-addition on Nb_3Sn layer formation remains ambiguous.

In this context, we have focused on the Sn diffusion driving force in Nb_3Sn formation. In general, the higher the Sn diffusion driving force, the higher the Nb_3Sn phase nucleation rate, which leads to a finer grain morphology. In the present study, we first confirm whether Hf addition, when compared with no Hf addition, induces grain refinement under a high Sn diffusion driving force. Here, we adopted Sn–10at%Cu as the core and examined the reaction behavior. We also compared the effects of Ta–Hf and Ti–Hf addition to Nb. Both Ta and Ti are well known as effective additives that increase B_{c2} [12][13]; however, in the case of enhancing B_{c2} by adding Ti to Nb, Ti can achieve the same effect as Ta when added in one-half the amount of Ta [14]. Therefore, in our experiments, we used Nb–4at%Ta and Nb–2at%Ti as base materials and compared the phase formation behavior of both materials with and without Hf addition. By analyzing the layer thickness, grain size, and composition in the Nb_3Sn layer, we revealed how the addition of Ta–Hf and Ti–Hf to the Nb core under a high Sn diffusion driving force affects Nb_3Sn formation.

II. EXPERIMENTAL

A. Samples

We prepared four samples with different diffusion couple structures. Four Nb alloys (i.e., Nb–4at%Ta, Nb–4at%Ta–1at%Hf, Nb–2at%Ti, and Nb–2at%Ti–1at%Hf) were

Submitted for review September 21, 2023
This work was supported in part by JSPS KAKENHI Grant Number JP23K04453. (Corresponding author: Nobuya Banno.)

Koki Asai is with Sophia University, Tokyo 102-8854, Japan, and with the National Institute for Materials Science, Tsukuba, Ibaraki 305-0047, Japan (e-mail: kouki0204@eagle.sophia.ac.jp)

Tsuyoshi Yagai is with the Sophia University, Tokyo 102-8554, Japan (e-mail: tsuyoshi-yagai@sophia.ac.jp).

Nobuya Banno is with the Research Center for Functional Materials, National Institute for Materials Science, Tsukuba, Ibaraki 305-0047, Japan (e-mail: banno.nobuya@nims.go.jp).

This work was partially supported by KAKENHI Grant number JP23K04453.

fabricated by an arc-melting process. These Nb alloys were cold-worked into a tube with an outer diameter of 5.8 mm and an inner diameter of 3.0 mm. Nb-alloy tubes were intermediately annealed at 900 °C for 5 h. A Sn alloy (Sn–10at%Cu) was inserted into the Nb-alloy tubes covered by Cu sheath, which were then swaged, die-drawn to a 1.09 mm-diameter wire, and rolled into a tape with a thickness of 0.23 mm. Cu is well known as a catalytic element to promote the Nb_3Sn layer formation [6]. Since the Cu penetration form the sheath into the Sn–Cu core through the tape ends was concerned, the Cu sheath was chemically etched before heat treatment. Microstructural observation on the end cross-section confirmed that there was no impact of acid etching on Sn–Cu. The heat treatment was carried out at 650 or 685 °C for 100 h to form the Nb_3Sn layer. The samples were named as follows:

(A) Nb–4Ta/Sn–10Cu
(B) Nb–4Ta–1Hf/Sn–10Cu
(C) Nb–2Ti/Sn–10Cu
(D) Nb–2Ti–1Hf/Sn–10Cu

No oxygen source was incorporated for any of the samples.

B. Microstructural and microchemical analyses

After the heat treatment, transverse cross-sections of the samples were observed by scanning electron microscopy (SEM). The overall layer thickness of Nb_3Sn and the ratio between the fine-grain layer thickness and the coarse-grain layer thickness were determined by averaging the typical thicknesses. The average grain size was calculated by dividing a given area by the number of grains in the area on the fractured microstructure in the fine-grain layer.

A composition analysis of the fine-grain Nb_3Sn layer was carried out by energy-dispersive X-ray spectroscopy (EDS).

III. Results

A. Nb_3Sn layer thickness

Fig. 1 shows SEM images of a cross-section of each sample. A thick layer of fine Nb_3Sn grains was formed at the forefront of the diffusion reaction, whereas a layer of course Nb_3Sn grains was formed at the Sn–Cu side through decomposition of Nb_6Sn_5.

Table 1 summarizes the overall layer thickness of Nb_3Sn and the ratio of the fine-grain layer thickness to the coarse-grain layer thickness. In the sample of Nb–4Ta/Sn–10Cu, cracks across the Nb outer sheath from the Sn–Cu core on the transverse cross-section were observed by SEM. That might result in somewhat thinner Nb_3Sn layer in Nb–4Ta/Sn–10Cu due to small Sn leakage through cracks. Focusing on the fine/coarse grain layer ratio, it was found that the fine layer tended to increase in samples to which Hf was added. In addition, irrespective of the presence of Hf, the fraction of fine layers increased in samples to which Ti was added compared with the fraction in samples to which Ta was added.

Compared to the fine/coarse grain layer ratio in samples prepared by the conventional manufacturing method, the ratios in samples prepared by the Tube-type method (2.67/1) and PIT method (4/1) are similar [15]. In these methods, Nb_3Sn is formed through a diffusion reaction between Nb and Nb_6Sn_5, like the Nb_3Sn formed in the present samples [11].

Table I. Overall Nb_3Sn layer thickness and fine/coarse grains layer ratio.

Sample	(A)	(B)	(C)	(D)
Addition to Nb-alloy	4Ta	4Ta-Hf	2Ti	2Ti-Hf
Layer thickness [Overall] (μm)	14.24	23.77	20.24	21.95
Fine grains layer thickness (μm)	8.23	15.93	14.49	16.26
The ratio of Fine/Coarse grains layer	1.37/1	2.03/1	2.52/1	2.86/1

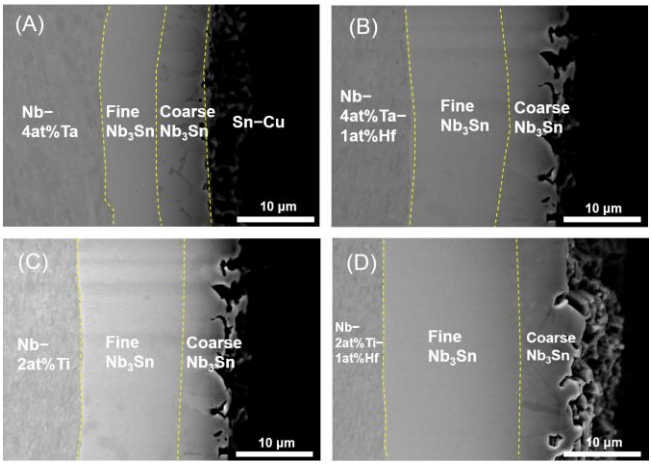

Fig. 1 Cross-sectional SEM images of reaction layer (acceleration voltage: 20 kV) for (a) Nb–4Ta/Sn–10Cu, (b) Nb–4Ta–1Hf/Sn–10Cu, (c) Nb–2Ti/Sn–10Cu, and (d) Nb–2Ti–1Hf/Sn–10Cu after diffusion for 100 h at 650 °C.

B. Nb_3Sn grain size

Fig. 2 shows fractured microstructure SEM images for samples (A)–(D). Grain morphologies in the Nb-side area, middle area, and Sn–Cu-side area in fine grain region were captured.

Table 2 summarizes the average Nb_3Sn grain size in the fine-grain layer. In all of the samples, the Nb_3Sn grain size was smallest at the reaction front with Nb. By contrast, in another study that used the RRP process, the grain size tended to increase near the interface with Nb [16]. In addition, in the bronze process, columnar coarse Nb_3Sn grains were observed at the Nb side [17]. The high Sn diffusion driving force might lead to refinement in the grain size at the reaction front.

Table II. Average Nb_3Sn grain size in fine-grain layers.

Sample	(A)	(B)	(C)	(D)
Addition to Nb-alloy	4Ta	4Ta-Hf	2Ti	2Ti-Hf
Grain size [Overall] (nm)	129.02	110.86	118.75	105.66
[Nb side] (nm)	125.20	105.72	103.30	97.38
[Middle] (nm)	134.04	111.22	119.16	108.44
[Sn-Cu side] (nm)	127.82	115.64	133.78	111.16

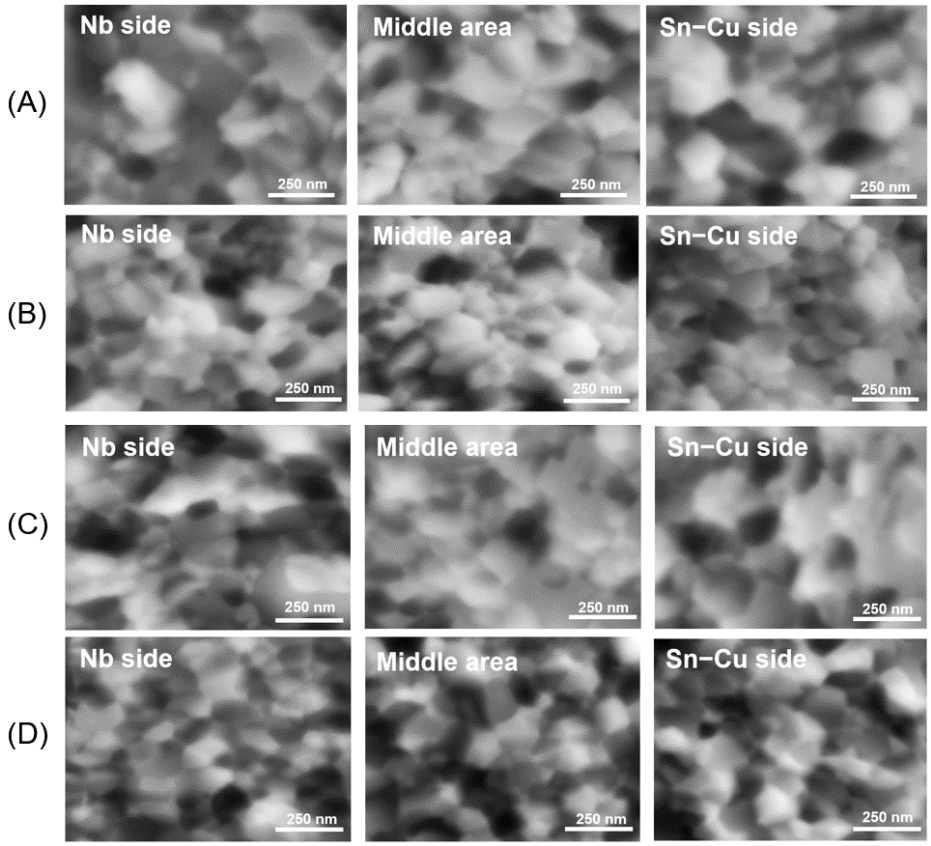

Fig. 2 Fractured cross-section SEM images (acceleration voltage: 10 kV) in fine grain region for (a) Nb–4Ta/Sn–10Cu, (b) Nb–4Ta–1Hf/Sn–10Cu, (c) Nb–2Ti/Sn–10Cu, (d) Nb–2Ti–1Hf/Sn–10Cu after diffusion for 100 h at 650 °C.

C. Composition profile in Nb_3Sn layer

Fig. 3 shows the Cu, Ta, and Ti compositional profiles (at%) in the layer of fine Nb_3Sn grains, as measured by EDS. The measurements were carried out at 20 points with equal distance along the straight line from the Nb side to Sn–Cu side in the fine grain layer. The Cu content appears to be higher with Hf addition than with only Ta or Ti addition. The reason for the higher Cu content in the samples with Ta addition than with Ti addition is unclear at the moment.

The Ta contents of sample (A) and (B) were almost the same to the original composition in the parent Nb–4Ta–1Hf, while the Ti contents of sample (C) and (D) were slightly smaller than the original composition. This trend might reflect the difference in the way of dissolving of Ta and Ti into Nb_3Sn lattice. As reported by Tarantini [18], Ta tends to sit on both the Nb and Sn sites in relatively low temperatures, whereas Ti sits only on the Nb site.

D. Influence of Nb_3Sn formation temperature

The heat-treatment temperature also significantly influences the Nb_3Sn phase formation. Fig. 4 shows a fractured cross-section near the reaction front of sample (A) heat-treated at 685 °C for 100 h. The cross-section shows intra-granular fracture. Some grains remained fine, whereas many grains grew substantially. The same tendency was observed in all the samples. A high Sn diffusion driving force appears to lead simultaneously to a high nucleation rate and to a high grain growth rate. For a high Sn diffusion driving

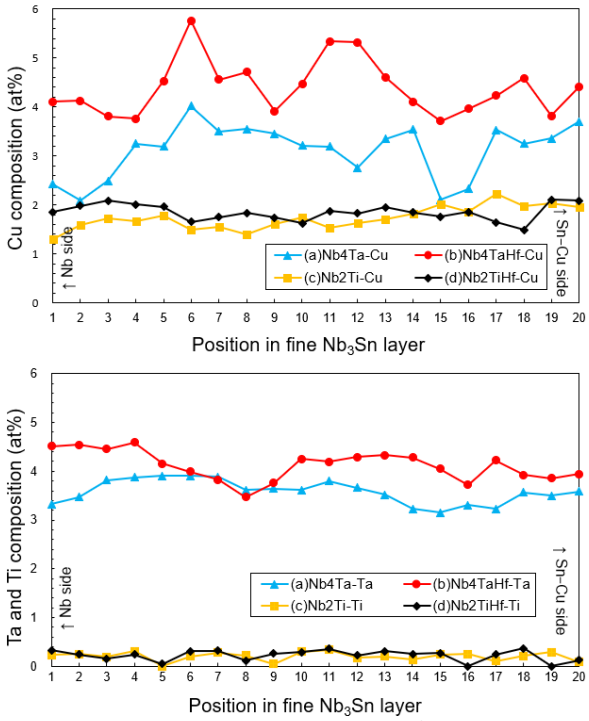

Fig. 3 Cu, Ta, and Ti content (at%) in the fine-grain Nb_3Sn layer characterized by EDS analysis (acceleration voltage: 20 kV). X-axis indicates the measurement point with equal distance in the fine grain region.

force, the heat-treatment temperature should be carefully optimized to obtain a fine-grain Nb_3Sn layer.

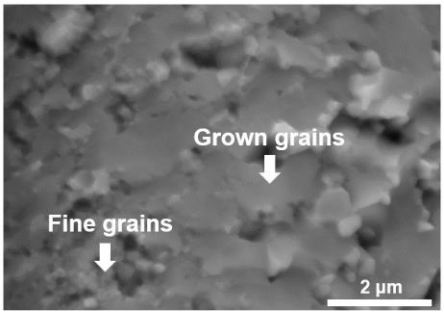

Fig. 4 The fractured cross-section SEM images for sample (A), Nb–4Ta/Sn–10Cu, heated at 685 °C for 100 h (acceleration voltage: 20 kV).

IV. Discussion

In both the Ta and Ti cases, the effect of Hf addition on grain refinement was observed under a high Sn diffusion driving force in the absence of an oxygen source. However, the effect of grain refinement by Hf addition appears to be weaker than expected on the basis of Balachandran et al.'s report [2] and also appreciably weaker than that reported by Xu et al. [10] for a PIT sample. The grain size was reduced by approximately 10-20% in this work in Hf-doping.

According to the Cu–Nb–Sn ternary phase diagram [19], when the Sn content in Sn–Cu is beyond 25at%, Nb_6Sn_5 is formed between Nb and Sn-Cu, and the formation of Nb_3Sn occurs through the diffusion reaction between Nb and Nb_6Sn_5. Therefore, the Nb_3Sn grain morphology could be almost determined by the difference of Sn chemical potential between the both phases. Hence, if the Sn concentration is higher than 25at%, the grain refinement effect is expected to be basically the same, even if the Sn concentration is lower, as in practical internal tin wires. On the contrast, in the case of bronze-route process, where Sn content Sn–Cu is far below 25at% and Nb_3Sn is directly formed, it is believed that Sn concentration strongly affects the Nb_3Sn formation behavior.

The grain refinement effect was slightly more appreciable in the case of Ti–Hf than Ta–Hf, inconsistent with our previously reported results [11]. Possible reasons for this could be the difference in Sn composition in the Cu-Sn phase and the reaction temperature. In order to rigorously compare the effects of Ti–Hf and Ta–Hf additions on the grain refinement, the effects of composition and temperature will need to be investigated, with either of those conditions fixed. In this work, we have already observed the microstructures of both samples after the heat treatment at 685 °C. However, the grain morphologies were too coarse to analyze. Appreciably, this temperature was too high at the condition with the Sn composition of 90% in the Cu–Sn. In the future, it will be necessary to analyze the change in grain morphology with annealing temperature in the case of lower Sn composition in Cu–Sn.

As is evident in Fig. 3, in cases of Ta and Ti doping, Hf addition led to a higher Cu content in Nb_3Sn compared to that without Hf addition. This difference was appreciable in the case of Ta. As noted in our recent work [11], Hf appears to have a strong affinity for Cu: Hf is likely to form a Cu–Hf compound at grain boundaries. The present result is consistent with this trend. In addition, the grain boundaries might be destabilized, leading to grain growth in the regions of higher Cu content on grain boundaries. Furthermore, a higher Nb_3Sn formation temperature in the bronze-route process would also facilitate grain growth. These effects might cancel out the effect of grain refinement by Hf addition.

In a recent study, Bovone *et al.* found that Hf addition without an oxygen source showed almost no effect on grain refinement [9]. The samples were fabricated by an RIT approach and had a multifilamentary assembly. In this assembly, Sn diffusion becomes complicated, making the weak effect of Hf addition on grain refinement difficult to determine.

V. Conclusion

In this study, we compared the effect of Ta–Hf and Ti–Hf addition to Nb under a high Sn diffusion driving force. First, we confirmed that the addition of Hf to Nb results in grain refinement for both Ta–Hf and Ti–Hf with no oxygen source. However, the grain refinement effect was smaller than that expected on the basis of previous works. Second, the grain size was smallest at the diffusion front with Nb. The high Sn diffusion driving force might cause this tendency. In addition, grain growth was observed after the heat treatment at 685 °C. The grain growth appeared to be sensitive to temperature in the case of a high Sn diffusion driving force.

References

[1] A. Ballarino and L. Bottura, "Targets for RandD on Nb_3Sn conductor for high energy physics," *IEEE Trans Appl Supercond*, vol. 25, no. 3, p. 6000906, Jun. 2015, doi: 10.1109/TASC.2015.2390149.

[2] S. Balachandran *et al.*, "Beneficial influence of Hf and Zr additions to Nb4at%Ta on the vortex pinning of Nb_3Sn with and without an O source," *Supercon Sci Technol*, vol. 32, no. 4, p. 044006, Feb. 2019, doi: 10.1088/1361-6668/aaff02.

[3] X. Xu, M. Sumption, X. Peng, and E. W. Collings, "Refinement of Nb_3Sn grain size by the generation of ZrO_2 precipitates in Nb_3Sn wires," *Appl Phys Lett*, vol. 104, no. 8, p. 082602, Feb. 2014, doi: 10.1063/1.4866865.

[4] X. Xu, X. Peng, J. Rochester, J.-Y. Lee, and M. Sumption, "High Critical Current Density in Internally-oxidized Nb_3Sn Superconductors and its Origin." *Scr Mater*, vol. 186, pp. 317–320, Sep. 2020, doi: 10.1016/j.scriptamat.2020.05.043.

[5] N. Banno, T. Morita, T. Yagai, and S. Nimori, "Influence of parent Nb-alloy grain morphology on the layer formation of Nb_3Sn and its flux pinning characteristics," *Scr Mater*, vol. 199, p. 113822, Jul. 2021, doi: 10.1016/j.scriptamat.2021.113822.

[6] N. Banno, "Low-temperature superconductors: Nb_3Sn, Nb_3Al, and NbTi," *Superconductivity*, vol. 6, p. 100047, Jun. 2023, doi: 10.1016/j.supcon.2023.100047.

[7] T. Morita, T. Yagai, and N. Banno, "Impact of Ti-doping position on Nb_3Sn layer formation in internal Sn-processed Nb_3Sn superconducting wires," *Cryogenics (Guildf)*, vol. 122, p. 103420, Mar. 2022, doi: 10.1016/j.cryogenics.2022.103420.

[8] N. Banno, T. Morita, T. Yagai, and S. Nimori, "Microstructure and Superconducting Properties of Hf-Ta Addition Bronze-Route Nb_3Sn

Wire," *IEEE Trans Appl Supercond*, vol. 32, no. 6, p. 600805, Sep. 2022, doi: 10.1109/TASC.2022.3160662.

[9] G. Bovone *et al.*, "Effects of the oxygen source configuration on the superconducting properties of internally-oxidized internal-Sn Nb_3Sn wires," *Supercond Sci Technol*, vol. 36, no. 9, p. 095018, Sep. 2023, doi: 10.1088/1361-6668/aced25.

[10] X. Xu, X. Peng, J. Rochester, J. Lee, G. Calderon Ortiz, and J. Hwang, "The strong influence of Ti, Zr, Hf solutes and their oxidation on microstructure and performance of Nb_3Sn superconductors," *J Alloys Compd*, vol. 857, p. 158270, Mar. 2021, doi: 10.1016/j.jallcom.2020.158270.

[11] N. Banno, T. Moronaga, T. Hara, K. Asai, and T. Yagai, "In-depth S/TEM observation of Ti-Hf and Ta-Hf-doped Nb_3Sn layers." Submitted to *Supercond. Sci. Technol.*

[12] K. Tachikawa, T. Asano, and T. Takeuchi, "High-field superconducting properties of the composite-processed Nb_3Sn with Nb-Ti alloy cores," *Appl Phys Lett*, vol. 39, no. 9, pp. 766–768, 1981, doi: 10.1063/1.92847.

[13] M. Suenaga and K. M. Ralls, "Some superconducting properties of Ti-Nb-Ta ternary alloys," *J Appl Phys*, vol. 40, no. 11, pp. 4457–4463, 1969, doi: 10.1063/1.1657215.

[14] M. Suenaga, "Optimization of Nb_3Sn," *IEEE Trans Magn*, vol. 21, no. 2, pp. 1122–1128, Mar. 1985, doi: 10.1109/TMAG.1985.1063633.

[15] X. Xu, "A review and prospects for Nb_3Sn superconductor development," *Supercond Sci Technol*, vol. 30, no. 9, p. 093001, Aug. 03, 2017, doi: 10.1088/1361-6668/aa7976.

[16] P. J. Lee and D. C. Larbalestier, "Microstructure, microchemistry and the development of very high Nb_3Sn layer critical current density," in *IEEE Trans Appl Supercond*, Jun. 2005, pp. 3474–3477, doi: 10.1109/TASC.2005.849064.

[17] D. Uglietti, V. Abächerli, M. Cantoni, and R. Flükiger, "Grain growth, morphology, and composition profiles in industrial Nb_3Sn wires," *IEEE Trans Appl Supercond*, Jun. 2007, pp. 2615–2618, doi: 10.1109/TASC.2007.898226.

[18] C. Tarantini *et al.*, "Ta, Ti and Hf effects on Nb_3Sn high-field performance: Temperature-dependent dopant occupancy and failure of Kramer extrapolation," *Supercond Sci Technol*, vol. 32, no. 12, p. 124003, Nov. 2019, doi: 10.1088/1361-6668/ab4d9e.

[19] J. Lachmann, M. J. Kriegel, A. Leineweber, S. L. Shang, and Z. K. Liu, "Thermodynamic re-modelling of the Cu–Nb–Sn system: Integrating the nausite phase," Calphad, vol. 77, Jun. 2022, Art. no. 102409, doi: 10.1016/j.calphad.2022.102409.